IOP Publishing Journal of Optics
J. Opt. **16** (2014) 094007 (8pp) doi:10.1088/2040-8978/16/9/094007

INVITED ARTICLE

Integrated terahertz multiparameter sensors using fiber/frequency selective surface couplers

Martin Girard and Maksim Skorobogatiy

Département de Génie Physique, École Polytechnique de Montréal, Montréal, H3C 3A7, Canada

E-mail: maksim.skorobogatiy@polymtl.ca

Received 1 April 2014, revised 24 July 2014
Accepted for publication 25 July 2014
Published 3 September 2014

Abstract

We propose using THz frequency selective surfaces interrogated with THz subwavelength optical fibers as integrated sensors for monitoring of the optical properties of thick optically non-transparent films that are brought into contact with such sensors. Changes in the test film thickness and absorption losses can be measured simultaneously by interpreting variations in the spectral resonant features in the fiber transmission and reflection spectra. In particular, changes in the film thickness induce strong shifts in the fiber transmission peaks, while changes in the film absorption induce notable amplitude variations in the fiber reflection peaks. When applied to the problem of monitoring the thickness and humidity content of paper sheets, the proposed system shows a sensitivity of 1.5 GHz/10 μm to changes in the paper's thickness and a sensitivity of 0.6/(% of water by volume) to changes in the paper's humidity. We estimate the detection limit of our device to be 10 μm for the paper thickness variation and 0.02% (of water by volume) for the paper humidity variation. The proposed sensor is implemented in the spirit of integrated optics, where a point device based on the frequency selective surface is interrogated with a THz fiber that is used for remote delivery of THz radiation.

Keywords: metamaterials, terahertz, fiber optics, spectroscopy, sensing

(Some figures may appear in colour only in the online journal)

1. Introduction

We have recently reported a theoretical study of transmission spectra of a subwavelength THz fiber that was evanescently coupled to a metasurface made of split ring resonators (SRR) deposited on a fused silica substrate [1]. Our original goal was to replace the traditional free-space THz time domain spectroscopy (THz-TDS) interrogation technique that is used to probe metasurfaces with a fiber-based system that would enable the remote delivery of optical power, as well as the interrogation of passive THz devices.

From our calculations, we find that transmission spectrum of a fiber that is evanescently coupled to a frequency selective surface (FSS) differs significantly from the transmission spectrum of a FSS measured perpendicular to its surface. In particular, a typical transmission spectrum through a SRR-patterned FSS shows a few relatively broad spectral features. In contrast, the transmission spectrum of a fiber coupled evanescently to FSS shows a large number of sharp (~1 GHz bandwidth) Fano resonances. To understand the nature of these peaks we note that a fiber coupled to a periodically patterned FSS presents by itself a periodic system. The corresponding modal structure of a fiber/FSS system can be analyzed using a folded band diagram of the optical states. Strong coupling between the THz fiber modes and those of a FSS results in a pronounced anti-crossing behavior, which also shows many flat regions in the dispersion relations of fiber/FSS hybrid modes. As is well known from the theory of

periodic optical systems, flat regions in the modal dispersion relations of guided modes are characterized by the significantly increased density of optical states and are known as Van Hove singularities. Finally, in our prior work [1], we show that the spectral position of the Fano resonances in the fiber transmission spectrum correspond exactly to the spectral position of the Van Hove singularities in the corresponding band diagram of an infinite fiber/FSS system.

As is the case with any sharp resonance, one can use changes in its spectral position and shape to monitor the properties of a measurand that is somehow coupled to the corresponding optical resonant state. For example, in [2] the authors use changes in the spectral position of Fano resonances as a sensing mechanism to identify recognition proteins monolayers adsorbed on a functionalized metasurface, at infrared frequencies. Recently, FSSs with high Q Fano resonances [3] were designed for possible applications in THz sensing with interrogation perpendicular to their surface.

In [1], we have shown the strong sensitivity of the Fano resonances in the fiber transmission spectrum to the fiber-metamaterial separation. Therefore, it is natural to question whether we can use fiber/FSS couplers with their sharp resonant features as a sensor. Currently, the fabrication of plastic THz fibers and SRR-patterned substrates is readily achieved using a variety of inexpensive fabrication techniques. Moreover, various moderately expensive THz sources have become widespread. In fact, one can use Time Domain Spectroscopy or Frequency Domain THz systems, or even economic single frequency THz sources, in order to profit from the fiber/FSS sensors described in this work.

Our work is motivated by the practical need for multi-parameter sensors that are capable of monitoring the various physical properties of thick (>10 μm) optically opaque layers (such as paper) where the traditional optical interference or spectroscopic techniques are unusable [4]. In particular, simultaneous characterization of paper thickness, density and humidity is an important industrial problem in paper manufacturing. Currently, one resorts to using several distinct sensors to do such a characterization, which requires a substantial integration engineering effort on the production line. Multiple sensors are typically integrated into scanning heads, which are then placed at various locations on the production line [5].

Paper thickness is usually measured using an electronic caliper, where two fingers are touching the paper, while the distance between the two fingers is determined by measuring the variable electric capacitance between the fingers. The precision of such a measurement can be very high, from 0.5–1 μm. However, this method has significant disadvantages. Since the paper sheet moves at high speeds (as high as 10 m s^{-1}), the fingers can tear the paper. Moreover, the fingers can polish the paper, producing a glossy stripe along the length, while also suffering wear from the mechanical contact with the paper.

In the case of water content, the measurement is typically performed by interpreting the transmission through paper of several distinct infrared wavelengths (usually 3 or 4) that are chosen to coincide with paper and water absorption lines. This is a non-contact characterization technique, which has a typical resolution of 0.25% of water by volume.

Given that the paper industry desires new sensors for quality control, such as fiber orientation, porosity, etc, the density of sensors in the production line will invariably increase. The multiplication of scanners is something that the industry wants to avoid, due both to the complexity of integration and maintenance, increased rates of failures, as well as to the added costs.

Recently, in [6] the authors reported using THz time domain spectroscopy (THz-TDS) to measure the thickness and absorption of paper films in a static configuration. This method profits from the relative transparency of paper to THz waves, and from the ability of a THz-TDS setup to simultaneously measure the amplitude and phase of the electric field transmitted through the paper film under test. In [6] the authors experimentally measure paper thickness with 0.5 μm precision, while the moisture content was measured with 0.25% (per weight) precision. The sensor system presented in [6] is essentially a classic THz-TDS setup that uses bulky free space optics in a highly precise arrangement, which can be challenging to maintain and service when installed on a real production line. In addition, the system can be prone to signal variations due to ambient humidity variations, unless the THz optics are sealed in a compartment with a controllable atmosphere. A similar characterization technique was recently used in [7], with the goal of characterizing water content in plants. In that work, many of the engineering challenges mentioned above were identified and successfully addressed, and the authors managed to build a functional hand-held system. Finally, the use of terahertz time-of-flight measurement has been suggested in [8], where the authors demonstrated the simultaneous measurement of the film refractive index and thickness with good precision; however, no absorption measurements were reported.

In this work we propose the use of fiber-metasurface coupler to simultaneously measure the thickness and water content of paper layers. Changes in the paper's thickness are monitored by registering spectral shifts of the peaks in the fiber transmission spectrum, while changes in the paper's humidity are interpreted from variations in the peak amplitudes in the fiber reflection spectrum. The main advantage of our system is that it can be used with any type of THz source (even an inexpensive single frequency source), thus avoiding the significant costs associated with a complete THz-TDS setup. Moreover, the integrated sensor can be easily packaged to avoid the influence of the environment.

2. Device geometry

The proposed device consists of a subwavelength fiber of radius R = 200 μm suspended in parallel over a FSS constructed by patterning split-ring resonators (SRR) on a 320 μm dielectric slab. The geometry is illustrated in figure 1, with geometrical parameters H = 25 μm, Λ = 400 μm, r = 90 μm, w = 15 μm and θ = 30°. The fiber is made of low-loss plastic, such as Polyethylene (n_{fiber} = 1.55), while the slab

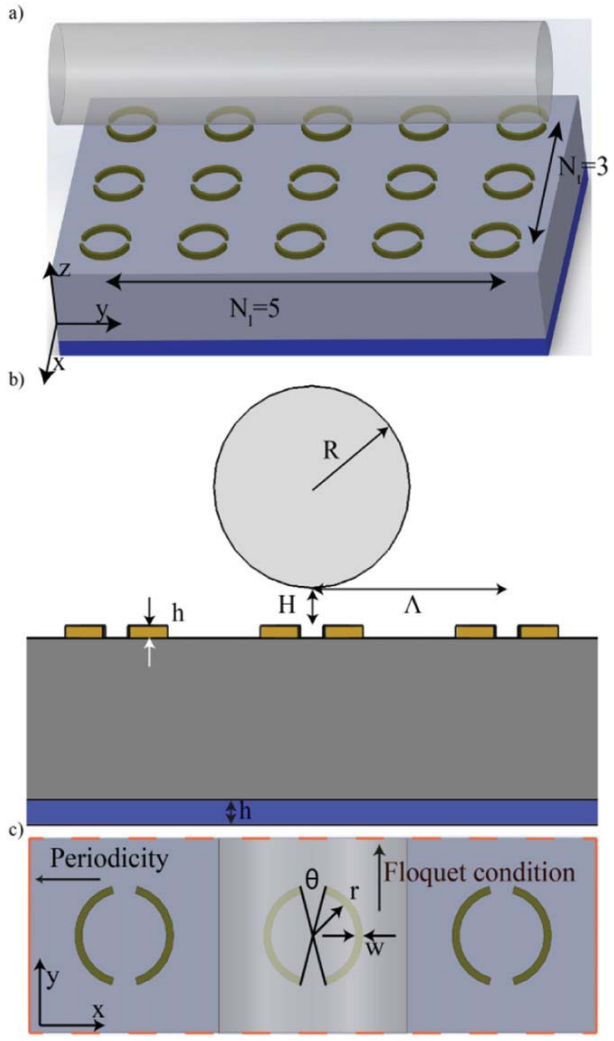

Figure 1. (a) 3D rendering of a subwavelength THz fiber interrogating a frequency selective surface featuring 5 periods in the longitudinal direction and 3 periods in the transversal direction. Test film of thickness h is placed in contact with the flat part of a substrate (one the opposite side from fiber). (b) Side view, c) top view of the unit cell, which corresponds to (a) and which we use in the band diagram calculations.

is made of fused silica ($n_{substrate} = 1.97$). The SRRs are assumed to be made of perfect electric conductors. The paper film under test is placed in direct contact with the FSS substrate. The SSR gaps are aligned with respect to the fiber direction, while the fiber is parallel to the SRR rows.

The Clausius-Mossotti model [9], along with liquid water permittivity measurements [10], as well as a double-Debye model [11] with Bruggeman effective medium [6] have been used to model the dielectric constant of paper in the presence of humidity.

A Bloch-Floquet condition is used for band diagram calculations to find the optical states in an infinitely long fiber/FSS structure. For finite structures, the port boundary condition is used with S-parameter calculations in order to compute fiber transmission and reflection spectra. COMSOL commercial finite element software is used in all calculations. For the port boundary conditions, we assume a single mode, at both the input waveguide and at the output waveguide, in the form of the fundamental HE_{11} fiber mode, which is linearly polarized along the z axis. A periodic boundary condition is imposed in the **x** direction to simulate an infinite metamaterial. A few millimeters of air are present over and under the system in the **z** direction and the computational cell is terminated with a PML.

The reason why this particular form of SRR was chosen and why this particular fiber direction was used is related to the ease of computation of the optical states associated with a coupled fiber/FSS system. In particular, if the fiber direction is parallel to the plane of a periodic FSS, and if the fiber is positioned within one of the FSS reflection symmetry planes, then the system is periodic along the fiber direction and the fiber/FSS optical states can be conveniently computed as Bloch states within the band diagram representation. Moreover, if the geometry of an individual SRR does not reduce the symmetry of an underlying FSS lattice (for example, SRR air gaps are aligned with respect to the FSS reflection symmetry planes), then Van Hove singularities in the optical density of states are especially easy to characterize. Indeed, in this case, such singularities are located along the high symmetry directions of the FSS reciprocal lattice and, therefore, only a one dimensional band diagram calculation is required. We remind the reader (for further details see [1]), that the spectral positions of the Van Hove singularities in the fiber/FSS optical density of states directly define the spectral positions of the resonant features in the fiber transmission spectrum. Since the amplitude and spectral changes associated with such transmission resonances constitute the main transduction mechanisms in the fiber/FSS sensor systems, our choices of SRR geometry and fiber direction were made specifically to simplify the computational effort related to characterization of performance of such sensors. It is possible that less symmetric fiber/FSS structures could provide higher sensitivities; however, the numerical analysis of such systems will be considerably more complex than that used in the current paper.

3. Fiber transmission and reflection spectra

In order to interpret the fiber transmission $t(f)$ and reflection $r(f)$ spectra, we use the scattering theory detailed in [12]. The scattering theory considers the interaction of N_r localized resonances with a single guided mode. In our case, the guided mode is the fundamental HE_{11} fiber mode and the resonances are the FSS substrate modes coupled to the fiber mode via split-ring resonators. For a system with lossy resonator states, we use a transfer matrix method [13], which requires us to solve the following equation:

$$\begin{pmatrix} t(f) \\ 0 \end{pmatrix} = M(f) \begin{pmatrix} 1 \\ r(f) \end{pmatrix}, \tag{1}$$

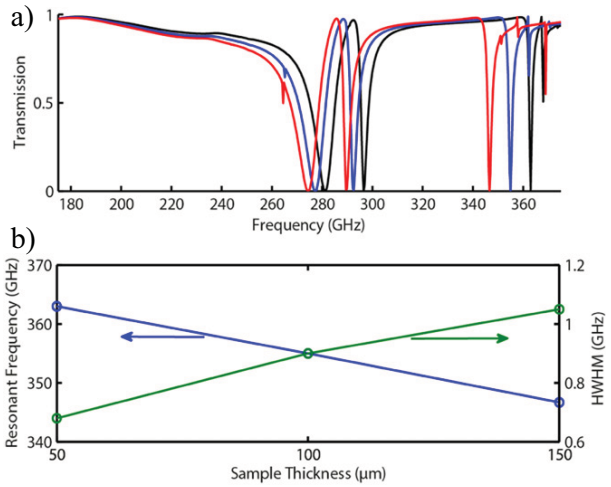

Figure 2. (a) Transmission through a subwavelength fiber coupled to a single cell of a FSS for various values of the paper's thickness $t = 50\,\mu$m (black), 100 μm (blue), 150 μm (red). (b) For the peak near 350 GHz, dependence of the peak parameters on the paper's thickness.

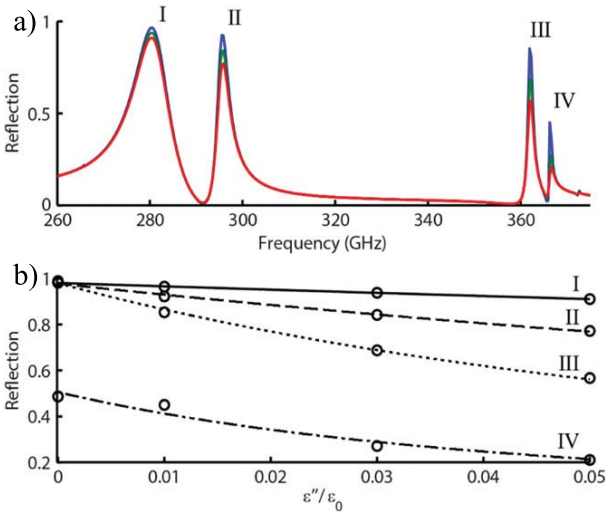

Figure 3. (a) Fiber reflection spectra for different values of the water content (by volume) w = 0.85%, $\varepsilon'' = 0.01$ (blue); w = 2.5%, $\varepsilon'' = 0.03$ (green); w = 4.1%, $\varepsilon'' = 0.05$ (red). (b) Value of the maximal reflection for four different resonances, I (solid), II (dashed), III (dotted), IV (dash-dotted), as a function of ε'' (paper thickness is fixed and equals to 50 μm).

where the transfer matrix $M(f)$ is defined by:

$$M(f) = \prod_{j=1}^{N_r} \begin{pmatrix} 1 - \dfrac{i\gamma_j}{f - f_j + i\Gamma_j} & -\dfrac{i\gamma_j}{f - f_j + i\Gamma_j} \\ \dfrac{i\gamma_j}{f - f_j + i\Gamma_j} & 1 + \dfrac{i\gamma_j}{f - f_j + i\Gamma_j} \end{pmatrix}. \quad (2)$$

Where f_j, γ_j and Γ_j are the resonant frequency, coupling strength, and losses that characterize the jth resonance. In particular, the resonant frequency corresponds to the phase matching point between the fiber and the FSS substrate modes, the coupling parameter is related to the resonance spectral width, while the loss parameter includes both the absorption losses introduced by the lossy paper film as well as radiation losses in the case of the leaky modes of a resonator. In the rest of this paper we disregard the absorption losses of the fiber material and the FSS substrate, which is a valid approximation at lower frequencies (below 0.5 THz), where the material losses of many dry dielectrics are small.

As we have mentioned earlier, variations in the paper thickness h changes geometry and modal properties of the FSS substrate. Thus, we expect that variations in this parameter can bring strong changes in the position of the fiber transmission resonances. In figure 2 we present the transmission spectra $T = |t|^2$ trough of a fiber suspended over a single period of a FSS ($N_l = 1$, $N_t = 3$, in figure 1) for various values of the paper's thickness $h = [50\,\mu\text{m}, 100\,\mu\text{m}, 150\,\mu\text{m}]$. In this simulation, we assume lossless paper $\Gamma = 0$, while the real part of the paper's permittivity is constant and equal to 2.25. Given that the paper's thickness varies, clear spectral shifts are observed in the position of the transmission peaks. The peak parameters can be extracted from the transmission spectra by fitting them with lineforms defined by (1) and (2). The largest frequency shift is produced by the peak near 350 GHz. We note that the peak spectral shift and the peak width (coupling parameter) depend linearly on paper thickness (see figure 2) in the studied parameter range. The spectral sensitivity, which is defined as a ratio of the frequency shift to the change in the layer thickness, is calculated to be as high as 1.6 GHz/10 μm.

We will now study changes in the fiber reflection spectrum when paper absorption loss is introduced. As follows from the lineshape (2), in the absence of losses, directly at the resonance, the reflection is perfect. When losses are introduced, the reflection coefficient at resonance decreases with increased losses Γ as:

$$R = |r|^2 = \frac{\gamma^2}{(\gamma + \Gamma)^2}. \quad (3)$$

This lineshape is only valid for a single resonance, and it should be modified when two or more resonances are found in the direct vicinity of this resonance.

Losses Γ in (3) can be varied by changing the imaginary part ε'' of the paper's permittivity. In figure 3(a) we show reflection spectra for $\varepsilon''/\varepsilon_0 = [0.01, 0.03, 0.05]$. These values for the ε'' of the humid paper correspond to the water content (by volume) of 0.85% to 4.1%, as calculated by assuming the Clausius-Mossotti model for the humid paper, and $\varepsilon''_w = 4.75$ for the bulk water [10].

In figure 3(a) we present dependence of the reflection peak shapes (labeled in figure 3(a) as I–IV) on paper losses. For each peak, lineshape (3) is used to fit the maximal value of the reflection as a function of the paper loss, where we assume that $\Gamma = C_\Gamma \cdot \varepsilon''$, where C_Γ is a fitting constant. An excellent agreement is found between the numerical results (circles in figure 3(b)) and analytical fitting with (3) (continuous curves in figure 3(b)). Interestingly, when increasing

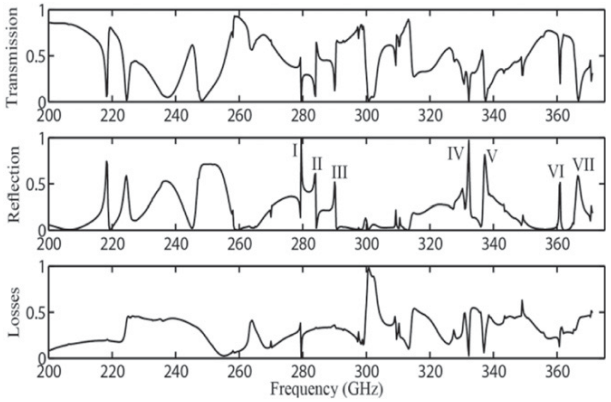

Figure 4. Interrogation of a longer section of FSS (10 periods) with a subwavelength fiber. (a) Transmission spectrum, (b) reflection spectrum, and (c) losses (1-R-T).

the paper losses, the maximal value of the reflection coefficient falls much faster for narrower peaks (which are characterized by smaller values of the coupling parameter γ). This is well in accordance with the form of lineshape (3). By defining sensitivity to changes in the water content as a derivative of the value of the reflection coefficient with respect to the water concentration (by volume), we conclude that a sensitivity as high as 0.08/(water % by volume) can be achieved at low humidity.

4. Band diagram versus S-parameter simulations

So far, we have presented the transmission and reflection spectra of a subwavelength fiber coupled to a single cell of a FSS. In figure 4 we present the transmission and reflection spectra for a subwavelength fiber coupled to a 10-period long section of a FSS. Compared to the case of a FSS with a single period, the spectra for a longer system features a much larger number of sharp resonances, typically with Fano lineshapes (for a detailed discussion of this phenomenon see our prior work [1]). This abundance of resonant peaks presents us with an opportunity to choose the peak with optimal parameters for the multiparameter detection modality. First of all, as we have mentioned earlier, using narrow resonances in reflection spectrum is advantageous for sensing changes in the paper losses. At the same time, one cannot use peaks with high radiative losses to determine water content (see for example spectral dips in the vicinity of 300 GHz in figure 4) because the change in the reflection coefficient would be too small to allow sensitive measurements. Moreover, the peak width should be larger than, while also being comparable to, the spectral resolution of a THz measurement setup. For example, in [14] we have experimentally demonstrated using the resonances of a THz fiber Bragg grating as narrow as 4 GHz, while using a THz-TDS setup with 1.5 GHz resolution (600 ps –long scans).

In what follows, we will, therefore, focus on the peaks that feature low radiative losses and spectral widths in the range of 1 GHz. Seven particular resonances (labeled as I–VII) have been chosen in figure 4 for further study.

To predict changes in spectral positions of the resonant peaks caused by variations in the paper's thickness, a direct approach would be to repeat the S-parameter calculations for each thickness value. However, this is not a viable proposition if long sections of FSS are used. For example, computing figure 4 took 80 GB of memory and five days of computation time. Therefore, a more robust method is required. One such method uses fast band diagram calculations (also known as the ω(k) method) to predict the positions of the resonant peaks in the fiber transmission spectra. As detailed in [1], the resonances seen in figure 4 correspond to Van Hove singularities in the band diagram of the optical states of an infinite fiber/FSS system. In figure 5(b) we demonstrate the band diagram method on an example resonance VI. In this figure the band diagrams are presented for various thicknesses of the paper's layers and the positions of Van Hove singularities that correspond to resonance VI are highlighted in dashed circles. The spectral positions of the resonances can then be tracked simply by plotting a series of band diagrams corresponding to the paper thicknesses of interest. This method is used to calculate the solid curves in figure 5(b). One can also confirm the validity of this approach by performing much longer S-parameter calculations. The results of these simulations for resonances VI and VII are presented as dashed lines. An excellent correspondence between the band diagram approach and an S-parameter approach is observed. Finally, by using data from figure 5(b), we can calculate spectral sensitivity of the peak position to changes in the paper's thickness for various resonances to be 0.8 GHz/10 μm, 1 GHz/10 μm, 1.1 GHz/10 μm, 1.1 GHz/10 μm, 0.85 GHz/10 μm, 1.5 GHz/10 μm and 1.6 GHz/10 μm for resonances I–VII, respectively. The above mentioned sensitivities are calculated as an average value of the derivative of the corresponding spectral peak shifts presented in figure 5 with respect to the paper thickness. The average is over three values of the paper thicknesses of 15 μm, 30 μm and 50 μm. It should be noted that, for most resonances, the shift in their spectral position is mostly linear with changes in the paper thickness (in the 0–85 μm paper thickness range). Notable exceptions are resonances III, IV and V. The reason for this is that the bands on which the Van Hove singularities are located move in frequency at a different rate than other adjacent bands. Due to interaction between these bands, they repulse each other in frequency and the displacement becomes non-linear.

Finally, we note that band diagram calculations (of the ω(k) type) cannot be used to directly compute the resonance loss parameter Γ. Therefore, changes in the reflection coefficient have to be calculated using an S-parameter method. In figure 6(a) we present the changes in the fiber reflection spectrum as a function of the paper loss (water content). As expected, higher paper losses result in smaller values of the reflection coefficient at resonance. To quantify this observation, in figure 6(b) we present maximal values of the reflection coefficient at various resonances (identified as I–VII in figure 4) as a function of the paper loss parameter $\varepsilon''/\varepsilon_0 = 0.01$, 0.03, 0.05. These values of the imaginary part of the paper's

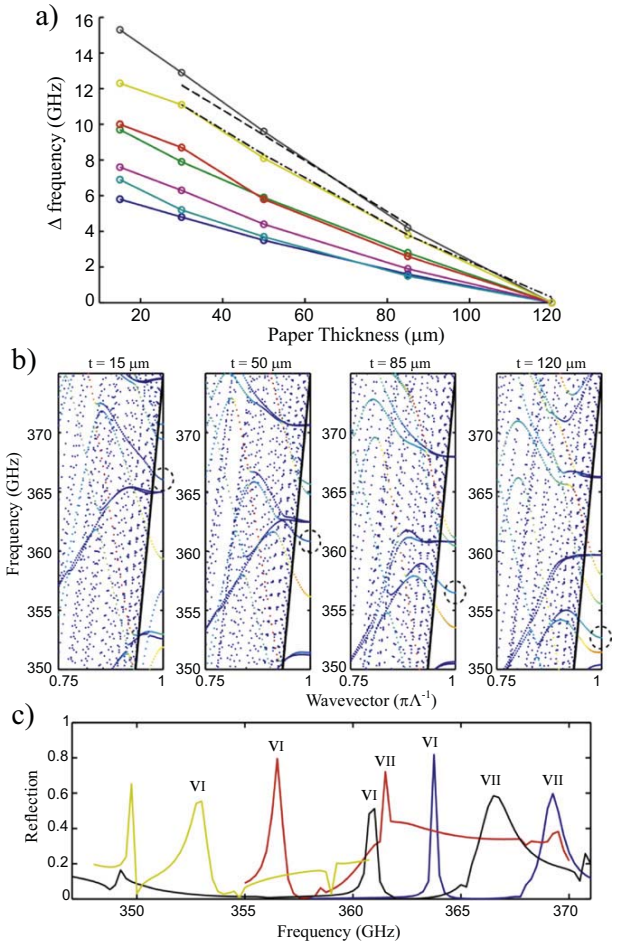

Figure 5. (a) Spectral change in the peak positions for different values of the paper thickness. Presented data is for resonances I (blue), II (green), III (red), IV (cyan), V (purple), VI (yellow), VII (black). In solid curves—results of the band diagram calculations, in dashed curves—results of the S-parameter calculation VI (dot-dashed) and VII (dashed). (b) Band diagrams of the optical states for an infinite fiber/FSS system for various values of paper thicknesses of 15 μm, 50 μm, 85 μm and 120 μm (resonance VI–dashed circles). (c) S-parameter calculations for resonances VI and VII for paper thicknesses of 30 μm (blue), 50 μm (black), 85 μm (red) and 120 μm (yellow) used to confirm results of (a) and (b). A clear change of peak shape is seen for resonance VII between thicknesses of 50 μm and 85 μm. The resolution step for calculations is 0.25 GHz in (a) and (c).

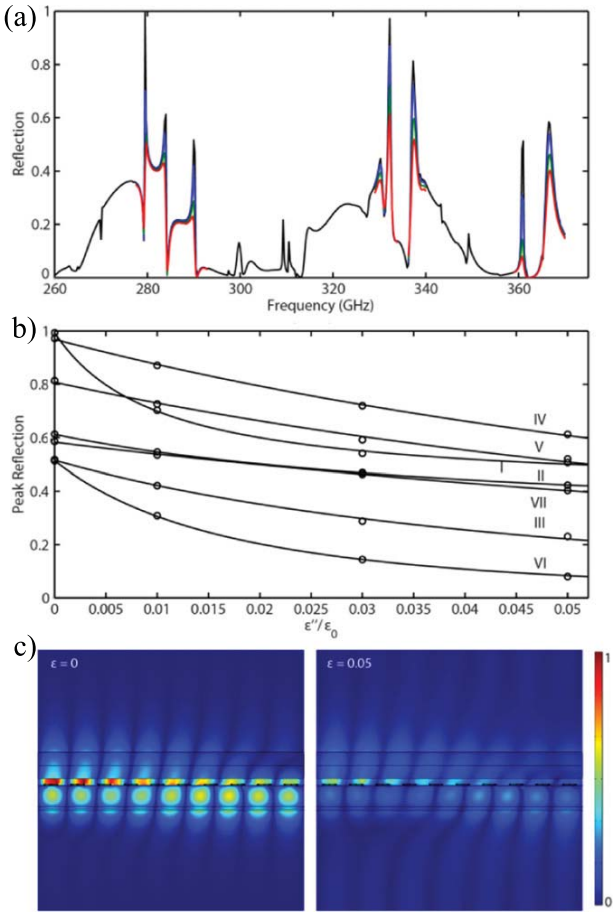

Figure 6. (a) Fiber reflection spectra calculated using S-parameter approach for different values of water content w = 0 (black), w = 0.85%, $\varepsilon''/\varepsilon_0 = 0.01$ (blue); w = 2.5%, $\varepsilon''/\varepsilon_0 = 0.03$ (green); w = 4.1%, $\varepsilon''/\varepsilon_0 = 0.05$ (red) and a fixed paper thickness of 50 μm. Reduction in the maximal values of the reflection coefficient at resonances is clearly visible when the paper loss increases. (b) Maximal value of the reflection coefficient for peaks I–VII. Circles —S-parameter calculations, solid curves—fitted lineshape (3). (c) field distributions calculated at the center frequency of resonance I using lossless films $\varepsilon'' = 0$ and lossy films $\varepsilon''/\varepsilon_0 = 0.05$.

permittivity correspond to the 0.85%, 2.5% and 4.1% of water by volume in the paper. Individual data points (circles in figure 6(b)) are then fitted with lineform (3) (solid cirves in figure 6(b)). An excellent fit is observed with a simple lineshape (3) for all of the resonances, except I and II. For these two resonances it is necessary to add a constant baseline to the lineshape (3) because they are too closely spaced with respect to each other and, therefore, a simple lineshape (3), which describes a single standing resonance, is no longer adequate. From the data in figure 6(b) we calculate that sensitivities as high as $52/(\varepsilon''/\varepsilon_0)$, or 0.60/(% water by water) can be achieved at low humidity levels (peak I). If we assume that a change of 1% of the reflectivity is measurable, then the limit of detection for water content is ~0.02%. This value can potentially be further decreased by using a thinner substrate but one has to consider experimental problems related to very thin substrates. Finally, in figure 6(c) we present electric field distributions calculated at the center frequency of resonance I for two different values of the film absorption coefficient $\varepsilon'' = 0$ and $\varepsilon''/\varepsilon_0 = 0.05$. The same injected power is used in both calculations. From these field distributions we can clearly see a significant impact of the film losses on the losses of a resonant mode.

While more resonant peaks could be found at higher frequencies, material absorption of the FSS substrate and fiber material also increases with frequency. For example, absorption for fused silica changes from ~0.25 cm^{-1} at 0.5 THz to ~1 cm^{-1} at 0.75 THz to ~2 cm^{-1} at 1 THz [15], while the absorption loss of polyethylene varies from

$\sim$0.1 cm^{-1} at 0.5 THz to $\sim$0.3 cm^{-1} at 1 THz [16]. As follows from the general considerations of the scattering theory (2), an increase in the material losses will significantly reduce the sensitivity of the resonances to changes in the paper loss when the resonance loss becomes comparable to the coupling strength parameter $\Gamma \sim \gamma$. Therefore, it is important at higher frequencies to take into consideration the material losses of the fiber/FSS system to produce a realistic analysis of sensor performance.

Other factors that can degrade system performance and reduce sensor sensitivity are related to various structural and material imperfections, such as the surface roughness of the fiber, substrate, and paper layer that induce additional losses. In a case when high losses (substrate absorption, scattering, etc) are present, using a resonance with a better sensitivity at high water content, such as resonance IV in figure 6, may prove to be a better choice. In that particular case, the maximum achievable LOD is of 0.14% of water content.

5. Discussion

In the previous section we saw that transmission and reflection spectra of a fiber coupled to FSS feature many sharp resonances. In transmission the changes in the spectral position of the resonances can be used to detect variations in the refractive index and thickness of the paper films. In reflection, changes in the resonance amplitude can be used to detect variations in the paper loss (water content). As seen in figures 4–6, there are a large number of resonances that can be used for detection. Therefore, it is important to ask about the optimal choice of working resonances that would optimize sensor performance.

When detecting variations in the paper thickness (figures 4, 5), one would generally use resonances that simultaneously exhibit large spectral shifts, as well as the linear dependence of such shifts with respect to changes in the paper thickness. In this respect, peaks VI and VII of figure 5 can be considered as optimal.

When detecting changes in the paper loss (water content), the optimal sensitivity is achieved with resonances that have the lowest inherent losses (see equation (3)). For example, from figure 3 it follows that peaks I, IV and V are among the best possible optimal choices to detect variations in the paper's losses. At the same time, resonance I shows the highly nonlinear dependence of its amplitude with paper loss. Therefore, using resonances IV and V is preferred from the point of view of ease of data interpretation.

In general, due to the different criteria used for the optimal choice of resonances, it seems that one has to use different resonant peaks for the optimal detection of paper thickness variations and losses. It is of interest for the future work to investigate whether, through design, the same resonance can be made optimal for both paper thickness and paper loss detection.

6. Conclusions

In conclusion, we have demonstrated a multiparameter sensor that uses THz subwavelength fiber to interrogate a THz frequency selective surface. The sensor is capable of simultaneous measurements of paper thickness and water content. The sensing principle is based on detection and analysis of changes in the fiber transmission and reflection spectra. Band diagram and S-parameter calculations are used to develop a robust theoretical foundation for analysis of the sensor performance. For the variations in the water content (paper humidity), sensitivities as high as 0.6/(% of water by volume) are predicted. The corresponding detection limit of 0.02% of water variation by volume is estimated by assuming that reliable detection of 1% change in the value of the reflection coefficient is possible. For the variations in paper thickness, sensitivities as high as 1.5 GHz/10 μm are predicted. The corresponding detection limit of 10 μm in paper thickness variation is estimated by assuming that the spectral resolution of a TDS-THz setup is 1.5 GHz. These values are superior to those previously reported for other types of metamaterial-based sensors of film thickness [17, 18]. Moreover, our sensor exhibits a virtually linear response over a wide range of thicknesses, while the sensors presented in [17, 18] show highly nonlinear exponential behavior. Although our sensor shows somewhat inferior sensitivity when compared to a direct THz-TDS-based thickness measurements detailed in [5], at the same time it also shows significantly higher sensitivities for the water content measurements. Furthermore, our approach does not require a coherent detection strategy and, therefore, much cheaper incoherent narrow-band sources and detector can be used. Finally, the proposed sensor is implemented in the spirit of integrated optics, where a point device based on the FSS is interrogated with a THz fiber that is used for remote delivery of THz radiation. We believe that this paradigm is advantageous for building modular, highly sensitive, while practical THz sensors.

References

[1] Girard M and Skorobogatiy M 2013 Probing terahertz metamaterials with subwavelength optical fibers *Opt. Express* **21** 14

[2] Wu C, Khanikaev A B, Adato R, Arju N, Altug H and Shvets G 2012 Fano-resonant asymmetric metamaterials for ultrasensitive spectroscopy and identification of molecular monolayers *Nature Mater.* **11** 69–75

[3] Cao W, Singh R, Al-Naib I A, He M, Taylor A J and Zhang W 2012 Low-loss ultra-high-Q dark mode plasmonic Fano metamaterials *Opt. Lett.* **37** 3366–8

[4] Buzea C and Robbie K 2005 State of the art in thin film thickness and deposition rate monitoring *Rep. Prog. Phys.* **68** 385–409

[5] Münch R 2013 Control systems for paper machines *Handbook of Paper and Board* ed H Holik (Weinheim: Wiley) pp 401–21

[6] Mousavi P, Haran F, Jez D, Santosa F and Dodge J S 2009 Simultaneous composition and thickness measurement of

paper using terahertz time-domain spectroscopy *Appl. Opt.* **48** 6541–6

[7] Jördens C, Scheller M, Breitenstein B, Selmar D and Koch M 2009 Evaluation of the leaf water status by means of the permittivity at terahertz frequencies *J. Biol. Phys.* **35** 255–64

[8] Hussain B, Ahmed M, Nawaz M, Saleem M, Razzaq M, Zia M A and Iqbal M 2012 Simultaneous determination of thickness and refractive index based on time-of-flight measurements of terahertz pulse *Appl. Opt.* **51** 5326–30

[9] Hattori T, Kumon H and Tamazumi H 2010 Terahertz spectroscopic characterization of paper *35th Int. Conf. Infrared Millimeter Terahertz waves (IRMMW-THZ)* pp 1–2

[10] Afsar M N and Hasted J B 1977 Measurements of the optical constants of liquid H_2O and D_2O between 6 and 450 cm^{-1} *J. Opt. Soc. Am.* **67** 902–4

[11] Vij J K, Simpson D R J and Panarina O E 2004 Far infrared spectroscopy of water at different temperatures: GHz to THz dielectric spectroscopy of water *J. Mol. Liq.* **112** 125–35

[12] Miroshnichenko A E, Flach S and Kivshar Y S 2010 Fano resonances in nanoscale structures *Rev. Mod. Phys.* **82** 2257–98

[13] Fan S H 2002 Sharp asymmetric line shapes in side-coupled waveguide-cavity systems *Appl. Phys. Lett.* **80** 908–10

[14] Yan G, Chiniforooshan Y, Mikulic P, Bock W and Skorobogatiy M 2013 Resonant THz sensor for paper quality monitoring using THz fiber Bragg gratings *Opt. Lett.* **38** 2200–2

[15] Grischkowsky D, Keiding S, Van Exter M and Fattinger C 1990 Far-infrared time-domain spectroscopy with terahertz beams of dielectrics and semiconductors *J. Opt. Soc. Am.* B **7** 2006–15

[16] Birch R, Dromey J D and Lisurf J 1981 The optical constants of some common low-loss polymers between 4 and 40 cm^{-1} *Infrared Phys.* **21** 225–8

[17] O'Hara J F, Singh R, Brener I, Smirnova E, Han J, Taylor A J and Zhang W 2008 Thin-film sensing with planar terahertz metamaterials: sensitivity and limitations *Opt. Express* **16** 1786–95

[18] Reinhard B, Schmitt K M, Wollrab V, Neu J, Beigang R and Rahm M 2012 Metamaterial near-field sensor for deep-subwavelength thickness measurements and sensitive refractometry in the terahertz frequency range *Appl. Phys. Lett.* **100** 221101